Hindawi Publishing Corporation
Abstract and Applied Analysis
Volume 2013, Article ID 171732, 7 pages
http://dx.doi.org/10.1155/2013/171732

Research Article

A Direct Eulerian GRP Scheme for the Prediction of Gas-Liquid Two-Phase Flow in HTHP Transient Wells

Jiuping Xu,[1] Min Luo,[1,2] Jiancheng Hu,[1,2] Shize Wang,[3] Bin Qi,[3] and Zhiguo Qiao[3]

[1] *Uncertainty Decision-Making Laboratory, Sichuan University, Chengdu 610064, China*
[2] *College of Mathematics, Chengdu University of Information Technology, Chengdu 610225, China*
[3] *Research School of Engineering Technology, China Petroleum and Chemical Corporation, Deyang 618000, China*

Correspondence should be addressed to Jiuping Xu; xujiuping@scu.edu.cn

Received 10 September 2013; Accepted 17 October 2013

Academic Editor: Mohamed Fathy El-Amin

A coupled system model of partial differential equations is presented in this paper, which concerns the variation of the pressure and temperature, velocity, and density at different times and depths in high temperature-high pressure (HTHP) gas-liquid two-phase flow wells. A new dimensional splitting technique with Eulerian generalized riemann problem (GRP) scheme is applied to solve this set of conservation equations, where Riemann invariants are introduced as the main ingredient to resolve the generalized Riemann problem. The basic data of "X well" (HTHP well), 7100 m deep, located in Southwest China, is used for the case history calculations. Curve graphs of pressures and temperatures along the depth of the well are plotted at different times. The comparison with the results of Lax Friedrichs (LxF) method shows that the calculating results are more fitting to the values of real measurement and the new method is of high accuracy.

1. Introduction

The prediction of pressure and temperature of transient gas-liquid flow in a wellbore is important but difficult for well completion test because they are characterized by the dependence of pressure, density, velocity, and other flow parameters on both time and space. As for pressure prediction research, there exist empirical formulas, such as those given by Beggs and Brill [1], Mukherjee and Brill [2, 3], and so on. Different researchers such as Hurlburt and Hanratty [4] and Cazarez-Candia and Vásquez-Cruz [5] have proposed mechanistic models, assuming that flow is under steady-state conditions; other researchers such as Taitel et al. [6]; Ouyang and Aziz [7] have proposed unsteady-state gas-liquid two-phase flow models. Fontanilla and Aziz [8] and Ali [9] presented two simultaneous ordinary differential equations for estimating the steam pressure and quality and solved these equations by using the fourth-order Runge-Kutta method. However, those models can only predict the pressure profiles but not the temperature profiles and ignored their interdependence.

Concerning both pressure and temperature in HTHP wells, Wu et al. have presented a coupled system model of differential equations in [10], but this model only considered the single phase flow statement. In this paper, we build a set of coupled partial differential equations of pressure, temperature, density, and velocity in HTHP gas-liquid two-phase flow wells on the base of the model which was build by Xu et al. in [11]. The numerical model, which accords with the actual situation of the well, allows for the change of oblique angle,different heat transfer medium in annular and the depth of the physical properties of the formation.

We found an algorithm solving model with generalized Riemann problem (GRP) scheme, which is an analytic extension of the Godunov scheme in [12] and originally designed by Li and Chen in [13] for the shallow water equations. A direct and simple derivation of the Eulerian generalized Riemann problem scheme is presented to get the integration in time of the conservation laws. Riemann invariants are applied in order to resolve the singularity at the jump discontinuity. The approach has the advantage that the contact discontinuity in each local wave pattern is always fixed with speed zero, while the rarefaction and the shock waves are located on either side. Since the extension of this scheme to multidimensional cases is obtained using

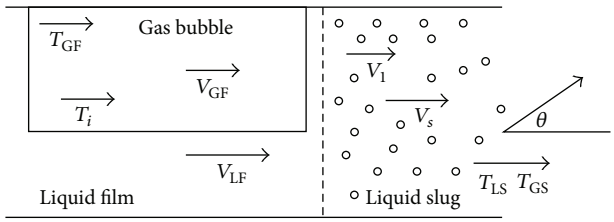

Figure 1: The two-phase flow.

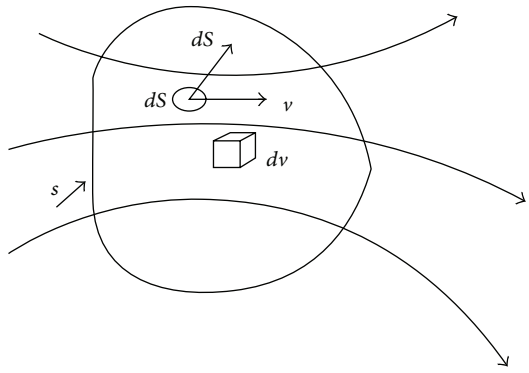

Figure 2: Control volume 1.

the dimensional splitting technique, getting the integration in time of the conservation laws is more direct and simple.

In this paper, we use GRP method for solving this problem and get more accurate prediction of pressure and temperature compared with those obtained from the existing correlations such as LxF method in [11]. The basic data for the calculation are from X well, 7100 m of depth in Southwest China. The curves of the gas pressure and temperature along the depth of the well are plotted. The results can provide a technical reliance for the process of designing well tests in HTHP gas-liquid wells and a dynamic analysis of production from wells.

2. Model Formulation

Considering the two-phase flow system shown in Figure 1, the mixture density and velocity are related to the in situ liquid volume fraction (holdup), H, as follows:

$$\begin{aligned} \rho_m &= \rho_l H + \rho_g (1 - H) \\ v_m &= v_l H + v_g (1 - H) \\ u_m &= u_l H + u_g (1 - H). \end{aligned} \tag{1}$$

2.1. Mass Balance. Consider the flow model shown in Figure 2. According to the fluid moves through the fixed control volume depicted by John and Anderson in [14], we have

$$\iint_S \rho_m v_m ds = -\frac{\partial}{\partial t} \iiint_v \rho_m dv_m. \tag{2}$$

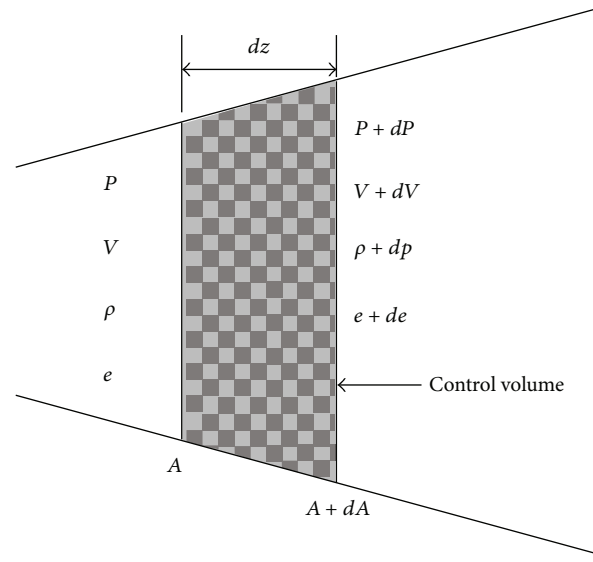

Figure 3: Control volume 2.

Under transient conditions, applied to the control volume in Figure 3, in the limit as dz becomes very small, the volume and surface integral in (2) becomes

$$\begin{aligned} \frac{\partial}{\partial t} \iiint_v \rho_m dv &= \frac{\partial}{\partial t} (\rho_m A dz) \\ \iint_S \rho_m v_m ds &= \rho_m v_m dv_m + \rho_m A dv_m + A v_m d\rho_m \\ &= d(\rho_m v_m A). \end{aligned} \tag{3}$$

Substituting (3) into (2), we get the mass balance equation:

$$\frac{\partial \rho_m}{\partial t} + \frac{\partial (\rho_m v_m)}{\partial z} = 0. \tag{4}$$

2.2. Momentum Balance. As shown in Figure 4, the integral form of the z component the momentum equation can be written as follows with the external forces:

$$\begin{aligned} &\frac{\partial}{\partial t} \iiint_v \rho_m u_m dV + \iint_S (\rho_m u_m v_m) \cdot dS \\ &\quad = -\iint_S (PdS)\, dz - \rho_m g \cos\theta A dz - \frac{\lambda \rho_m v_m^2}{2d} A dz, \end{aligned} \tag{5}$$

where $\rho_m g \cos\theta A dz$ is the force of gravity, $(\lambda \rho_m v^2 A/2) dz$ is the shear stress, and

$$\begin{aligned} \frac{\partial}{\partial t} \iiint_v \rho_m u_m dV &= \frac{\partial}{\partial t} (\rho_m v_m A dz) \\ \iint_S (\rho_m u_m v_m) \cdot dS &= -\rho_m v_m^2 A \\ &\quad + (\rho_m + d\rho_m)(v_m + dv_m)^2 (A + dA) \\ -\iint_S (PdS)_z &= -PA + (P + dP)(A + dA) - 2P\left(\frac{dA}{2}\right). \end{aligned} \tag{6}$$

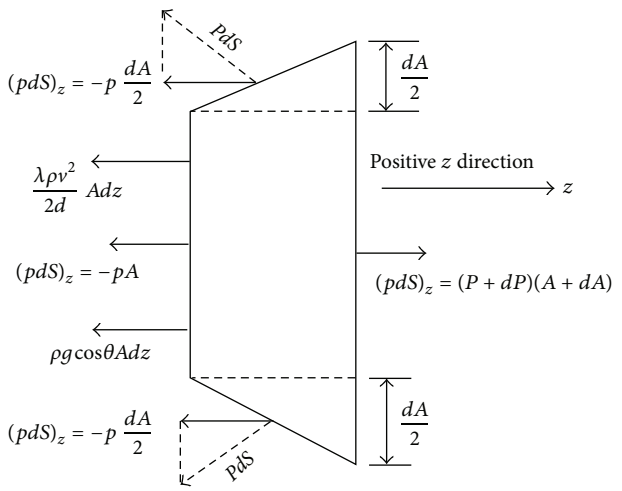

Figure 4: Control volume 3.

Substituting (6) into (5), we obtain momentum balance equation:

$$\frac{\partial}{\partial t}\left(\rho_m v_m\right) + \frac{\partial}{\partial z}\left(P + \rho_m v_m^2\right) = -\rho_m g\cos\theta - \frac{\lambda\rho_m v_m^2}{2d}. \quad (7)$$

2.3. Energy Balance. For the transient flow, it leads directly to the energy equation in terms of temperature. As shown in Figure 5, we should consider the heat transmission within wellbore and from wellbore to formation as transient.

According to the energy balance law, the heat variation flowing on control volume that is equal to the combination heat of inflow and outflow, and the heat transferring to the second dimension, we get the energy balance equation of transient flow:

$$\begin{aligned}&\left(wC_pT\right)z - \left(wC_pT\right)(z+dz) - 2\pi r_{to}U_{to}\left(T - T_r\right)dz \\ &\quad = \frac{\partial\left(\rho_m C_p T\right)}{\partial t}Adz,\end{aligned} \quad (8)$$

where $T_r = (K_e T_{ei} + r_{to}U_{to}T_e T_{\mathrm{wbD}})/(K_e + r_{to}U_{to}T_{\mathrm{wbD}})$ and $w = \rho_m v_m A$. Equation (8) equals the following equation:

$$\frac{\partial\left(\rho_m v_m T\right)}{\partial z} + \frac{\partial\left(\rho_m T\right)}{\partial t} = \frac{2\pi K_e r_{to}U_{to}\left(T_{ei} - T\right)}{C_P\left(K_e + r_{to}U_{to}T_{\mathrm{wbD}}\right)}. \quad (9)$$

Finally, we obtain the coupled system model of partial differential equations:

$$\begin{aligned}&\frac{\partial\rho_m}{\partial t} + \frac{\partial\left(\rho_m v_m\right)}{\partial z} = 0,\\ &\frac{\partial\left(\rho_m v_m\right)}{\partial t} + \frac{\partial\left(P + \rho_m v_m^2\right)}{\partial z} = -\rho_m g\cos\theta - \frac{\lambda}{2d},\\ &\frac{\partial\left(\rho_m T\right)}{\partial t} + \frac{\partial\left(\rho_m v_m T\right)}{\partial z} = \frac{2\pi K_e r_{to}U_{to}\left(T_{ei} - T\right)}{C_P\left(K_e + r_{to}U_{to}T_{\mathrm{wbD}}\right)},\\ &\rho_m = \frac{MP\gamma_g}{ZRT},\\ &\left(P, T, \rho_m, v_m\right) = \left(P_0, T_0, \rho_{m0}, v_{m0}\right) \quad t = 0,\ z = 0.\end{aligned} \quad (10)$$

3. Format Construction

We unify the conservation equations (4), (7), and (9) which are also included in (10) into the following formation:

$$\begin{aligned}&\frac{\partial A_m}{\partial t} + \frac{\partial B_m}{\partial z} = C_m, \quad m = 1, 2, 3,\\ &U = \begin{cases}A_1 = \rho_m\\ A_2 = \rho_m v_m\\ A_3 = 0,\end{cases} \qquad F(U) = \begin{cases}B_1 = \rho_m v_m\\ B_2 = P + \rho_m v_m^2\\ B_3 = \rho_m v_m T,\end{cases}\\ &S(U) = \begin{cases}C_1 = 0\\ C_2 = -\rho_m g\cos\theta - \dfrac{\lambda}{2d}\\ C_3 = \dfrac{2\pi K_e r_{to}U_{to}\left(T_{ei} - T\right)}{C_P\left(K_e + r_{to}U_{to}T_{\mathrm{wbD}}\right)}.\end{cases}\end{aligned} \quad (11)$$

We define the equally spaced grid points, the interface points, and the cells as

$$z_j = j\Delta z, \qquad z_{j+1/2} = \frac{z_j + z_{j+1}}{2}, \qquad C_j = \left[z_{j-1/2}, z_{j+1/2}\right]. \quad (12)$$

We assume that the data at time $t = t_n$ are piecewise linear with a slope σ_j^n and we have $U(z, t_n) = U_j^n + \sigma_j^n(z - z_j)$, $z \in (z_{j-1/2}, z_{j+1/2})$.

The second-order Godunov scheme for (11) takes the following form: $U_j^{n+1} = U_j^n - (\Delta t/\Delta x)(F(U_{j+1/2}^{n+1/2}) - F(U_{j-1/2}^{n+1/2}))$, where $U_{j+1/2}^{n+1/2}$ is the midpoint value or the value of U at the cell interface $(z_{j+1/2}, t_n)$ with accuracy of second order. More specifically, the mid-point value $U_{j+1/2}^{n+1/2}$ is computed with the formulas $U_{j+1/2}^{n+1} = U_{j+1/2}^n + (\Delta t/2)\left(\partial U/\partial t\right)_{j+1/2}^n$ and $U_{j+1/2}^n = R^A(0; U_{j+1/2,-}^n, U_{j+1/2,+}^n)$. Also, $R^A((z - z_{j+1/2})/(t - t_n); U_{j+1/2,-}^n, U_{j+1/2,+}^n)$ is the solution of the Riemann problem centered at $(z_{j+1/2}, t_n)$. Moreover, $U_{j+1/2,-}^n$ and $U_{j+1/2,+}^n$ are the limiting values of initial data $U(z, t_n)$ on both sides of $(z_{j+1/2}, t_n)$. We present a direct and simple derivation of the Eulerian geralized Riemann problem (GRP) scheme and apply Riemann invariants in order to resolve the singularity at the jump discontinuity.

The local wave configuration is usually piecewise smooth and consists of rarefaction waves, shocks, and contact discontinuities. As the general rarefaction waves are considered, the initial data can be regarded as a perturbation of the Riemann initial data U_L and U_R.

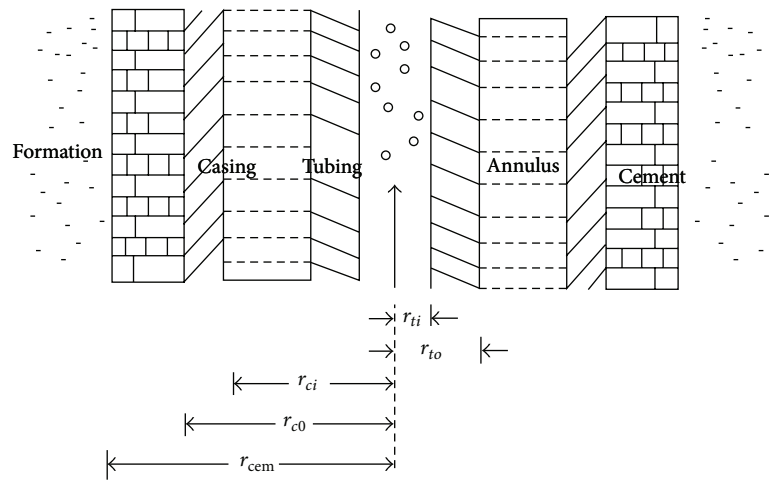

FIGURE 5: The radial transfer of heat.

The GRP scheme assumes piecewise linear data for the flow variables, which leads to the generalized Riemann problem for (11) subject to the initial data:

$$U(z,0) = \begin{cases} U_L + zU_L', & z < 0 \\ U_R + zU_R', & z > 0, \end{cases} \tag{13}$$

where U_L, U_R, U_L', and U_R' are constant vectors.

The initial structure of the solution is determined by the associated Riemann solution, denoted by $\lim_{t\to 0} U(\lambda t, t) = R^A(\lambda; U_L, U_R)$, $\lambda = x/t$.

4. Solving Process

Step 1. Set the step length. In this paper,

$$h = 1\ (\mathrm{m}), \qquad \tau = 60\ (\mathrm{s}). \tag{14}$$

Step 2. Obtain each point's inclination: $\theta_j = \theta_{j-1} + (\theta_{j'} - \theta_{j'-1})h/\Delta s_{j'-1}$.

Step 3. The in situ liquid volume fraction (holdup) in (1) can be calculated from

$$H(\theta_j) = \frac{0.98 E_l^{0.4846}}{Fr^{0.0868}} \times \left\{ 1 + (1 - E_l) \ln \left[\frac{4.7 N_{vl}^{0.1244}}{E_l^{0.8692} Fr^{0.5056}} \right] \times \left[\sin(1.8\theta_j) - \frac{1}{3}\sin^3(1.8\theta_j) \right] \right\}. \tag{15}$$

Step 4. Calculate the following parameters by Liao and Feng in [15]:

$$U_{to} = \left(\frac{r_{to}}{r_{ti} h_r} + \frac{r_{to} \ln(r_{to}/r_{ti})}{r_{ti} h_r} + \frac{1}{h_c + h_r} + \frac{r_{to} \ln(r_{c0}/r_{ci})}{r_{\mathrm{cas}}} + \frac{r_{to} \ln(r_h/r_{c0})}{r_{\mathrm{cem}}} \right)^{-1},$$

$$T_{\mathrm{wbD}} = \frac{2\pi K_e (T_{ei} - T_{\mathrm{wb}})}{\sum_{j=1}^{m} (Q_{j-1} - Q_j)}. \tag{16}$$

Step 5. For piecewise given initial data $U^n(z) = U_j^n + \sigma_j^n (z - z_j)$, $z \in (z_{j-1/2}, z_{j+1/2})$, we solve the Riemann problem for (11) to define the Riemann solution $U_{j+1/2}^n = R(0; U_j^n + (\Delta z/2)\sigma_j^n, U_{j+1}^n - (\Delta z/2)\sigma_{j+1}^n)$, which is the same as the classical Godunov scheme and the Riemann solver in [16] is used in the solution.

Step 6. Determine $(\partial U/\partial t)_{j+1/2}^n$ and evaluate the new cell averages U_j^{n+1}. We apply monotonic algorithm slope limiters to suppress the local oscillations near discontinuities. We use parameter $\alpha = 1.9$ in $\sigma_j^{n+1} = \min\mathrm{mod}(\alpha(U_j^{n+1} - U_{j-1}^{n+1})/\Delta z, \sigma_j^{n+1,-}, \alpha(U_{j+1}^{n+1} - U_j^{n+1})/\Delta z)$, where $U_{j+1/2}^{n+1,-} = U_{j+1/2}^n + \Delta z(\partial U/\partial z)_{j+1/2}^n$ and $\sigma_j^{n+1,-} = (1/\Delta z)(\Delta U)_j^{n+1,-} = (1/\Delta z)(U_{j+1/2}^{n+1,-} - U_{j-1/2}^{n+1,-})$.

5. Results and Discussion

In this simulation, we study a pipe in X well located in Sichuan Basin, Southwest China. All the needed parameters are given in [17] as follows: fluid density is 1000 kg/m^3; depth of the well is 7100 m; friction coefficient is 1.2; ground temperature is 160°C; ground thermal conductivity parameter is 2.06; ground temperature gradient is 0.0218°C/m. Parameters of pipes are given in Table 1. Inclination, azimuth, and vertical depth are given in Table 2.

Through the simulation, we use GRP method to calculate the prediction of pressure and temperature of the oil in the pipe and draw a sensitive analysis for the results. We compare the results of pressure and temperature calculated for the well head at 1200 s by GRP and LxF scheme with the measurement results, which also shows that GRP scheme is more accurate

Table 1: Parameters of pipes.

Diameter	Thickness	Weight	Expansion	Coefficient	Young	Modulus
88.9	9.53	18.9	0.0000115	215	0.3	1400
88.9	7.34	15.18	0.0000115	215	0.3	750
88.9	6.45	13.69	0.0000115	215	0.3	4200
73	7.82	12.8	0.0000115	215	0.3	600
73	5.51	9.52	0.0000115	215	0.3	150

Table 2: Parameters of azimuth, inclination, and vertical depth.

Number	Measured	Inclination	Azimuth	Vertical depth
1	0	0	120.33	0
2	303	1.97	121.2	302.87
3	600	1.93	120.28	599.73
4	899	0.75	126.57	898.59
5	1206	1.25	124.9	1205.45
6	1505	1.04	124.62	1504.32
7	1800	0.49	123.75	1799.18
8	2105	2.49	125.27	2104.04
9	2401	1.27	123.13	2399.91
10	2669	2.44	120.12	2667.79
11	3021	0.14	127.39	3019.63
12	3299	1.18	122.60	3297.50
13	3605	2.05	123.25	3603.36
14	3901	0.16	121.45	3899.22
15	4183	2.92	121.24	4181.09
16	4492	2.73	129.22	4489.95
17	4816.07	1.98	121.61	4813.87
18	5099.07	2.74	129.93	5096.74
19	5394.07	0.13	120.46	5391.61
20	5706.07	0.63	129.59	5703.47
21	5983.07	2.09	120.14	5980.34
22	6302.07	2.69	122.91	6299.19
23	6597.07	2.45	129.41	6594.06
24	6911.12	0.15	124.88	6907.96

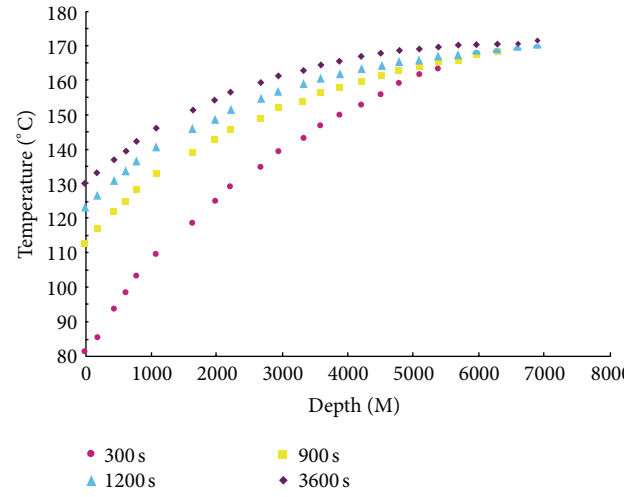

Figure 6: Temperature distribution at different depths.

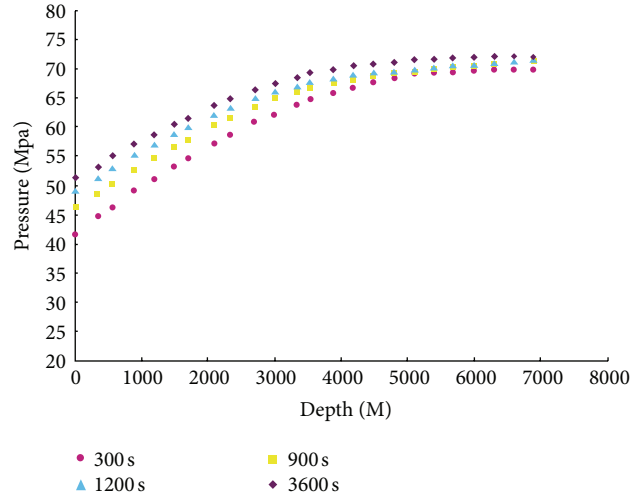

Figure 7: Pressure distribution at different depths.

in the real calculation. We obtain series of results contained in tables and figures and analyze these results as follows.

When the bottom pressure is 70 MPa, temperatures are plotted in Figure 6 at different depths and shown in detail in Table 3. When the output keeps constant, the temperature increases with the increasing depth of the well and when the depth fixed, the temperature increases with the increasing time. In addition, it can be seen from the figure that the temperature changes quickly in the early stage but stabilizes over time, especially after 1200 s.

It is established that, when depth is constant, the pressure shown in Figure 7 and Table 4 increased with an increase of the time. When the output keeps constant, the pressure increased with the increasing depth of the well. This is because, with time increasing, the flow increases and then the frictional heat leads to an increase in the pressure. It can also be seen that the pressure changes quickly in the early stage but stabilizes over time.

As shown in Table 5, for the comparative results of the well head temperature at 1200 s, the relative error between the calculation results and the measurement results of GRP scheme method is 5.12% and by LxF method is 6.70%, while the relative error between the results in pressure predition at

Table 3: Temperature at different depths on 300 s, 900 s, 1200 s, and 3600 s.

Depth	Time			
	300 s	900 s	1200 s	3600 s
0	81.22	115.29	124.19	132.27
300	85.45	121.38	127.55	133.34
600	92.67	125.54	131.76	136.56
900	95.54	129.48	134.96	138.87
1200	101.16	133.77	137.58	141.94
1500	106.49	136.66	140.77	143.15
1800	111.76	140.67	143.23	145.17
2100	116.98	143.54	146.29	147.39
2400	121.86	145.66	148.49	149.14
2700	126.89	148.45	150.78	151.93
3000	131.55	151.78	152.99	153.85
3300	136.85	153.74	154.86	155.91
3600	140.88	154.02	154.46	157.87
3900	144.67	157.12	158.73	159.45
4200	148.25	159.34	160.87	161.88
4500	152.74	161.53	161.65	162.65
4800	155.77	162.55	162.72	163.45
5100	159.75	163.42	163.49	164.56
5400	162.36	164.56	164.87	165.24
5700	164.32	165.74	165.45	166.57
6000	166.36	166.56	167.67	167.97
6300	167.91	168.77	168.87	169.65
6600	168.23	169.45	169.57	169.81
6900	170.24	170.56	171.78	171.52

Table 4: Pressure at different depths on 300 s, 900 s, 1200 s, and 3600 s.

Depth	Time			
	300 s	900 s	1200 s	3600 s
0	42.55	46.62	50.24	51.34
300	43.23	47.53	50.64	52.67
600	44.86	48.71	50.46	53.47
900	45.87	49.13	51.41	54.69
1200	46.73	50.43	52.32	54.79
1500	48.46	51.24	53.36	55.53
1800	49.43	52.43	54.47	56.12
2100	50.34	53.83	55.42	57.37
2400	51.96	56.92	54.37	57.85
2700	53.53	57.22	55.45	58.97
3000	54.44	58.46	56.78	59.34
3300	55.24	59.97	57.47	60.95
3600	56.76	59.94	58.95	61.22
3900	57.33	60.98	59.04	62.29
4200	58.93	61.22	60.29	63.33
4500	59.34	62.45	61.24	64.48
4800	60.89	63.43	62.23	64.33
5100	61.56	64.19	63.22	64.78
5400	63.35	65.24	64.18	65.34
5700	64.69	65.45	65.12	66.34
6000	65.45	66.79	66.15	67.56
6300	66.99	67.49	67.11	67.47
6600	67.46	68.52	68.22	68.58
6900	69.28	69.46	69.92	69.55

the same time calculated by GRP scheme method is 8.81% and by LxF method is 9.73%, which shows that the distribution prediction of the two-phase flow is more accurate in actual calculation by GRP scheme method.

6. Conclusion

In this paper, considering the variation of pressure, temperature, velocity; and density at different times and depths in gas-liquid two-phase flow, we present a system model of partial differential equations according to mass, momentum, and energy. We establish an algorithm solving model with a new difference method with a direct Eulerian GRP scheme which is proven to be efficient for the numerical implementation in this paper. The basic data of the X well (HTHP well), 7100 m deep in Sichuan Basin, Southwest China, was used for case history calculations, and a sensitivity analysis is completed for the model. The gas-liquid's pressure and temperature curves along the depth of the well are plotted, and the curves intuitively reflect the flow law and the characteristics of heat transfer in formation. The results can provide the technical reliance for the process of designing well tests in high temperature-high pressure gas-liquid two-phase flow wells and dynamic analysis of production. Furthermore, the works in this paper can raise safety and reliability of deep completion test and will yield notable economic and social benefits and avoid or lessen accidents caused by improper technical design.

Table 5: Comparative results of the well head at 1200 s.

Well-head	Temperature	Pressure
Measurement results	180.65	76.10
Results by GRP method (relative error)	171.78 (5.12%)	69.92 (8.81%)
Results by LxF method (relative error)	169.30 (6.70%)	69.36 (9.73%)

Nomenclature

A: A total length of conduit (m^2)
C_J: Joule-Thompson coefficient (K/pa)
C_p: Heat capacity (J/kg·K)
D: A hydraulic diameter (m)
G: Acceleration constant of gravity (m/s^2)
K_e: Formation conductivity (J/m·K)
P: Pressure (KPa)
r_D: Dimensionless radius
r_{to}: Outer radius of conduit (m)
T: Temperature (K)
t_D: Dimensionless time

T_e: Temperature of the stratum (K)
T_{wb}: Wellbore temperature (K)
T_{wbD}: Dimensionless wellbore temperature (K)
T_r: Temperature of the second surface (K)
T_{ei}: Initial temperature of formation (K)
U_{to}: Overall-heat-transfer coefficient (W/m·K)
V: Velocity (m/s)
Z: A total length of conduit (m)
z: The distance coordinate in the direction along the conduit
h_c: Heat transfer coefficient for natural convection based on outside tubing surface and the temperature difference between outside tubing and inside casing surface
h_r: Heat transfer coefficient for radiation based on the outside tubing surface and the temperature difference between the outside tubing and inside casing surface
K_{cas}: Thermal conductivity of the casing material at the average casing temperature
K_{cem}: Thermal conductivity of the cement at the average cement temperature and pressure
λ : The friction coefficient, dimensionless
γ_g: Euler constant 1.781
ρ : Density (kg/m^3)
θ : Inclination angle flow conduit.

Conflict of Interests

The authors declare that there is no conflict of interests regarding the publication of this paper.

Acknowledgments

This research was supported by the Key Program of NSFC (Grant no. 70831005) and the Key Project of China Petroleum and Chemical Corporation (Grant no. GJ-73-0706).

References

[1] H. D. Beggs and J. R. Brill, "A study of two-phase flow in inclined pipes," *Journal of Petroleum Technology*, vol. 25, pp. 607–617, 1973.

[2] H. Mukherjee and J. P. Brill, "Liquid holdup correlations for inclined two-phase flow," *Journal of Petroleum Technology*, vol. 35, no. 5, pp. 1003–1008, 1983.

[3] H. Mukherjee and J. P. Brill, "Empirical equations to predict flow patterns in two-phase inclined flow," *International Journal of Multiphase Flow*, vol. 11, no. 3, pp. 299–315, 1985.

[4] E. T. Hurlburt and T. J. Hanratty, "Prediction of the transition from stratified to slug and plug flow for long pipes," *International Journal of Multiphase Flow*, vol. 28, no. 5, pp. 707–729, 2002.

[5] O. Cazarez-Candia and M. A. Vásquez-Cruz, "Prediction of pressure, temperature, and velocity distribution of two-phase flow in oil wells," *Journal of Petroleum Science and Engineering*, vol. 46, no. 3, pp. 195–208, 2005.

[6] Y. Taitel, O. Shoham, and J. P. Brill, "Simplified transient solution and simulation of two-phase flow in pipelines," *Chemical Engineering Science*, vol. 44, no. 6, pp. 1353–1359, 1989.

[7] L.-B. Ouyang and K. Aziz, "Transient gas-liquid two-phase flow in pipes with radial influx or efflux," *Journal of Petroleum Science and Engineering*, vol. 30, no. 3-4, pp. 167–179, 2001.

[8] J. P. Fontanilla and K. Aziz, "Prediction of bottom-hole conditions for wet steam injection wells," *Journal of Canadian Petroleum Technology*, vol. 21, no. 2, 8 pages, 1982.

[9] S. M. F. Ali, "A comprehensive wellbore stream/water flow model for steam injection and geothermal applications," *Society of Petroleum Engineers Journal*, vol. 21, no. 5, pp. 527–534, 1981.

[10] Z. Wu, J. Xu, X. Wang, K. Chen, X. Li, and X. Zhao, "Predicting temperature and pressure in high-temperature-high-pressure gas wells," *Petroleum Science and Technology*, vol. 29, no. 2, pp. 132–148, 2011.

[11] J. Xu, M. Luo, S. Wang, B. Qi, and Z. Qiao, "Pressure and temperature prediction of transient flow in HTHP injection wells by Lax-Friedrichs method," *Petroleum Science and Technology*, vol. 31, no. 9, pp. 960–976, 2013.

[12] S. K. Godunov, "A difference method for numerical calculation of discontinuous solutions of the equations of hydrodynamics," *Matematicheskii Sbornik*, vol. 47, no. 89, pp. 271–306, 1959.

[13] J. Li and G. Chen, "The generalized Riemann problem method for the shallow water equations with bottom topography," *International Journal for Numerical Methods in Engineering*, vol. 65, no. 6, pp. 834–862, 2006.

[14] D. John and J. R. Anderson, *Computational Fluid Dynamics—The Basics with Applications*, McGraw-Hill, New York, NY, USA, 1995.

[15] X.-W. Liao and J.-L. Feng, "Pressure-temperature coupling calculation of transient wellbore heat transfer in deep geopressured gas reservoir," *Petroleum Exploration and Development*, vol. 32, no. 1, pp. 67–69, 2005.

[16] E. F. Toro, *Riemann Solvers and Numerical Methods for Fluid Dynamics: A Practical Introduction*, Springer, Berlin, Germany, 1997.

[17] J. Xu, J. Hu, M. Luo, S. Wang, B. Qi, and Z. Qiao, "Optimisation of perforation distribution in HTHP vertical wells," *Canadian Journal of Chemical Engineering*, vol. 91, pp. 332–343, 2011.